

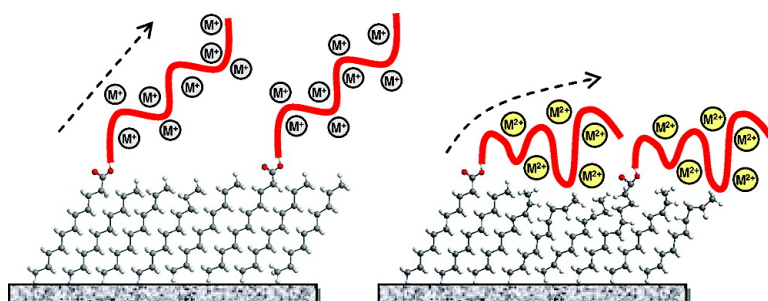
Article

Metal Cation-Induced Deformation of DNA Self-Assembled Monolayers on Silicon: Vibrational Sum Frequency Generation Spectroscopy

Hidehiko Asanuma, Hidenori Noguchi, Kohei Uosaki, and Hua-Zhong Yu

J. Am. Chem. Soc., **2008**, 130 (25), 8016-8022 • DOI: 10.1021/ja801023r • Publication Date (Web): 03 June 2008

Downloaded from <http://pubs.acs.org> on February 8, 2009



More About This Article

Additional resources and features associated with this article are available within the HTML version:

- Supporting Information
- Links to the 2 articles that cite this article, as of the time of this article download
- Access to high resolution figures
- Links to articles and content related to this article
- Copyright permission to reproduce figures and/or text from this article

[View the Full Text HTML](#)



ACS Publications
 High quality. High impact.

Metal Cation-Induced Deformation of DNA Self-Assembled Monolayers on Silicon: Vibrational Sum Frequency Generation Spectroscopy

Hidehiko Asanuma,[†] Hidenori Noguchi,[‡] Kohei Uosaki,^{*,‡} and Hua-Zhong Yu^{*,†}

Department of Chemistry, Simon Fraser University, Burnaby, British Columbia V5A 1S6, Canada, and Division of Chemistry, Graduate School of Science, Hokkaido University, Sapporo 060-0180, Japan

Received February 9, 2008; E-mail: hogan_yu@sfu.ca; uosaki@pcl.sci.hokudai.ac.jp

Abstract: Nucleic acids possess charged phosphate groups in their backbones, which require counterions to reduce the repulsive Coulombic interactions between the strands. Herein we report how different mono- and divalent metal cations influence the molecular orientations of DNA molecules on silicon surfaces upon immobilization and hybridization. Our sum frequency generation (SFG) spectroscopy studies demonstrated that the degree of conformational variation of DNA self-assembled monolayers on silicon depends on the type of metal cations present. The molecular orientation change of immobilized single-stranded oligonucleotides correlates with DNA–cation affinity ($Mg^{2+} > Ca^{2+} > K^+ \sim Na^+$): metal cations with the strongest affinity disrupt the structure of the underlying linker monolayer the most. Upon hybridization the trend is reversed, which is attributed to the greater ability of divalent cations to mask the negative charges on the DNA backbone. These findings provide useful information for the construction of more sensitive DNA biosensors, particularly the optimization of on-chip hybridization performance.

1. Introduction

DNA helices are negatively charged polyelectrolytes associated with cations that reduce the repulsive Coulombic interactions between the phosphate groups within and between the strands. The cations may induce deformation (bending, twisting, and changing of groove widths) as well as condensation of DNA strands even at short lengths.^{1–3} The type, concentration, and hydration degree affect their affinities for the binding sites and play a crucial role in governing the structure, stability, and reactivity of nucleic acids (DNA/RNA).^{2–12} In the past, extensive experimental and theoretical investigations have been carried

out with solvated and crystalline DNA,^{1–14} but little is known to date about the influence of different cations on the molecular conformations and on the hybridization reactivity of oligonucleotide strands immobilized on solid surfaces.

DNA monolayers on various substrates (e.g., gold¹⁵ and silicon^{16–21}) prepared via self-assembly are essential for the fabrication of chip-based DNA biosensors.^{22–24} The attachment of oligonucleotides onto oxide-free silicon has attracted considerable attention because crystalline semiconductors are atomically flat and their surface structures are well-defined. This eventually permits the use of existing microelectronics technology for the fabrication and testing of semiconductor-based

[†] Simon Fraser University.

[‡] Hokkaido University.

- (1) Hud, N. V.; Polak, M. *Curr. Opin. Struct. Biol.* **2001**, *11*, 293–301.
- (2) McFail-Isom, L.; Sines, C. C.; Williams, L. D. *Curr. Opin. Struct. Biol.* **1999**, *9*, 298–304.
- (3) Williams, L. D. *Annu. Rev. Biophys. Biomol. Struct.* **2000**, *29*, 497–521.
- (4) Allahyarov, E.; Gompper, G.; Lowen, H. *Phys. Rev. E* **2004**, *69*, 041904.
- (5) Allahyarov, E.; Lowen, H.; Gompper, G. *Phys. Rev. E* **2003**, *68*, 061903.
- (6) Anderson, C. F.; Record, M. T. *Annu. Rev. Phys. Chem.* **1995**, *46*, 657–700.
- (7) Andresen, K.; Das, R.; Park, H. Y.; Smith, H.; Kwok, L. W.; Lamb, J. S.; Kirkland, E. J.; Herschlag, D.; Finkelstein, K. D.; Pollack, L. *Phys. Rev. Lett.* **2004**, *93*, 248103.
- (8) Cerda, B. A.; Wesdemiotis, C. *J. Am. Chem. Soc.* **1996**, *118*, 11884–11892.
- (9) Korolev, N.; Lyubartsev, A. P.; Rupprecht, A.; Nordenskiold, L. *Biophys. J.* **1999**, *77*, 2736–2749.
- (10) Savelyev, A.; Papoian, G. A. *J. Am. Chem. Soc.* **2006**, *128*, 14506–14518.
- (11) Subirana, J. A.; Soler-Lopez, M. *Annu. Rev. Biophys. Biomol. Struct.* **2003**, *32*, 27–45.
- (12) Tan, Z. J.; Chen, S. J. *Biophys. J.* **2006**, *90*, 1175–1190.

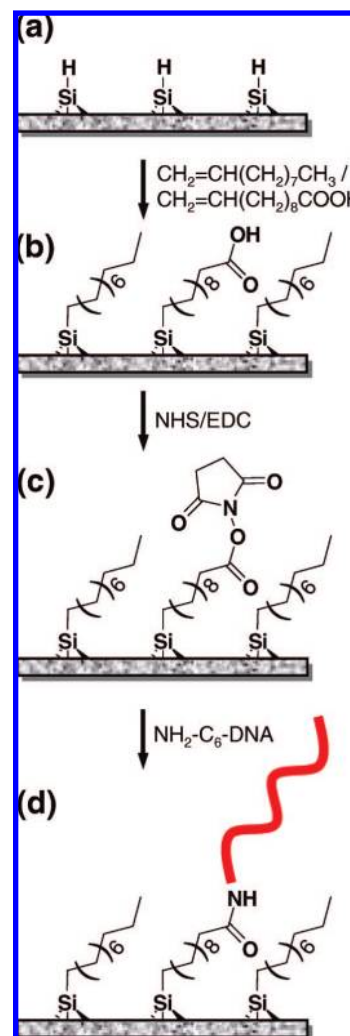
- (13) Korolev, N.; Lyubartsev, A. P.; Rupprecht, A.; Nordenskiold, L. *J. Phys. Chem. B* **1999**, *103*, 9008–9019.
- (14) Russo, N.; Toscano, M.; Grand, A. *J. Phys. Chem. A* **2003**, *107*, 11533–11538.
- (15) Herne, T. M.; Tarlov, M. *J. Am. Chem. Soc.* **1997**, *119*, 8916–8920.
- (16) Cai, W.; Peck, J. R.; Weide, D. W. v. d.; Hamers, R. J. *Biosens. Bioelectron.* **2004**, *19*, 1013–1019.
- (17) Pike, A. R.; Lie, L. H.; Eagling, R. A.; Ryder, L. C.; Patole, S. N.; Connolly, B. A.; Horrocks, B. R.; Houlton, A. *Angew. Chem., Int. Ed.* **2002**, *41*, 615–617.
- (18) Strother, T.; Cai, W.; Zhao, X. S.; Hamers, R. J.; Smith, L. M. *J. Am. Chem. Soc.* **2000**, *122*, 1205–1209.
- (19) Voicu, R.; Boukherroub, R.; Bartzoka, V.; Ward, T.; Wojtyk, J. T. C.; Wayner, D. D. M. *Langmuir* **2004**, *20*, 11713–11720.
- (20) Yin, H. B.; Brown, T.; Greef, R.; Wilkinson, J. S.; Melvin, T. *Microelectron. Eng.* **2004**, *73–74*, 830–836.
- (21) Yin, H. B.; Brown, T.; Wilkinson, J. S.; Eason, R. W.; Melvin, T. *Nucleic Acids Res.* **2004**, *32*, e113.
- (22) Pike, A.; Horrocks, B.; Connolly, B.; Houlton, A. *Aust. J. Chem.* **2002**, *55*, 191–194.
- (23) Pirrung, M. C. *Angew. Chem., Int. Ed.* **2002**, *41*, 1276–1289.
- (24) Xiao, Y.; Piorek, B. D.; Plaxco, K. W.; Heeger, A. J. *J. Am. Chem. Soc.* **2005**, *127*, 17990–17991.

biochips.^{25,26} According to the protocol reported by Strother et al.,¹⁸ single-stranded DNA (ssDNA) can be electrostatically immobilized via cross-linker molecules on ω -carboxyl monolayers on silicon. Later, covalent anchoring was proposed, either by the formation of amide linkages to amine-functionalized DNA^{16,20,21} or by on-chip DNA synthesis starting from an ω -undecanol monolayer.¹⁷ These pioneering studies have focused on DNA attachment strategies, surface patterning methods, and detection techniques.^{16–21} In contrast, relatively little is known about the structure and physical behavior of DNA molecules and their interactions on silicon surfaces. We therefore reasoned that a thorough investigation would be of practical value for the optimization of DNA hybridization arrays²³ and the design of other types of DNA-based biosensors.²⁴

In order to investigate the conformations of immobilized DNA strands on microarray chips, surface-sensitive techniques capable of revealing molecular order must be employed. Herein, we explore the application of sum frequency generation (SFG) spectroscopy to probe the structure and behavior of DNA self-assembled monolayers (SAMs) on silicon, in particular the effect of metal cations on the immobilization and hybridization processes. SFG spectroscopy is based on a second-order nonlinear optical effect of a photon generated at a frequency equal to the sum of the frequencies of two incident light beams, often infrared and visible, to induce specific vibrations at buried interfacial sites. According to the electric dipole approximation, second-order optical effects are prohibited in media exhibiting inversion symmetry; therefore, SFG is an extremely sensitive technique capable of revealing molecular conformations at interfaces.^{27–29} Stokes et al.³⁰ have recently communicated their SFG investigation of monolayers formed on glass from DNA strands rich in thymine (e.g., poly-AT). In such cases, the investigation of cation–DNA interactions is not feasible because the binding of counterions is sequence-specific.¹

Our approach is to monitor the underlying linker layer instead of the rather weak signals generated by the DNA strands directly, which allows us to probe any sequence of interest. In particular, a carboxyl-terminated linker monolayer was prepared by reacting hydrogen-terminated silicon ($\equiv\text{Si-H}$) with a mixture of 1-decene [$\text{CH}_2=\text{CH}(\text{CH}_2)_7\text{CH}_3$] and undecylenic acid [$\text{CH}_2=\text{CH}(\text{CH}_2)_8\text{COOH}$], to which amino-terminated DNA strands were attached via amide coupling.¹⁹ SFG is extremely sensitive to methyl groups at the surface: for example, it can be used to monitor the surface hydrolysis reactions of ester-terminated monolayers.³¹ In the mixed monoalyers, the n -alkyl chains will essentially act as excellent “molecular probes”. We expected that the structure of this underlying mixed monolayer would be disturbed if the immobilized DNA strands experienced substantial conformational changes. In other words, by examining the molecular order of the alkyl chains in the linker monolayer, we would be able to reveal the structural properties

Scheme 1. Preparation of DNA SAMs on Silicon



of DNA SAMs on silicon upon immobilization and after hybridization.

2. Experimental Section

2.1. Materials. All chemicals were of ACS reagent-grade quality and were used as received, unless otherwise stated. Deionized water (Milli-Q, $>18.3 \Omega \cdot \text{cm}$) was used throughout the experiments. 1-Decene (94%), undecylenic acid (98%), N -hydroxysuccinimide (NHS), 1-ethyl-3-(3-dimethylaminopropyl)carbodiimide hydrochloride (EDC), and 1,1,1-trichloroethane (99.5%) were purchased from Aldrich Japan (Tokyo, Japan); tetrahydrofuran (THF), methanol (99.0%), ethanol (99.0%), propanol (99.0%), sulfuric acid (96%), and hydrogen peroxide (30%) were from Wako Pure Chemical Industries (Osaka, Japan); and ammonium fluoride (40%) was from Morita Chemical Industries (Osaka, Japan). The amine-functionalized oligonucleotide [$5' \text{-NH}_2 \text{-(CH}_2)_6 \text{-TCGATCTGACGTCAGTC-AAA-3'}$] and the complementary strand ($3' \text{-AGCTAGACTGCAGTCAGTTT-5'}$) were ordered from Sigma Genosys Japan (Tokyo, Japan). 1-Decene was distilled from sodium under reduced pressure (20–30 Torr); undecylenic acid was purified by passage through an activated Al_2O_3 column.

2.2. Surface Preparation. The procedure for the surface preparation (attachment of linker layer, surface activation, and immobilization of single-stranded DNA) is shown in Scheme 1. Silicon (111) wafers ($3.0\text{--}5.0 \Omega \cdot \text{cm}$, n -type, donated by Shin-Etsu Semiconductors, Tokyo, Japan) were cut into pieces ($1.5 \times 2 \text{ cm}^2$) and cleaned in “piranha” solution (3:1 mixture of concentrated

(25) Boukherroub, R. *Curr. Opin. Solid State Mater. Sci.* **2005**, *9*, 66–72.

(26) Wagner, P.; Nock, S.; Spudich, J. A.; Volkmuth, W. D.; Chu, S.; Cicero, R. L.; Wade, C. P.; Linford, M. R.; Chidsey, C. E. D. *J. Struct. Biol.* **1997**, *119*, 189–201.

(27) Messmer, M. C.; Conboy, J. C.; Richmond, G. L. *J. Am. Chem. Soc.* **1995**, *117*, 8039–8040.

(28) Richmond, G. L. *Chem. Rev.* **2002**, *102*, 2693–2724.

(29) Shen, Y. R. *Nature* **1989**, *337*, 519–525.

(30) Stokes, G. Y.; Gibbs-Davis, J. M.; Boman, F. C.; Stepp, B. R.; Condie, A. G.; Nguyen, S. T.; Geiger, F. M. *J. Am. Chem. Soc.* **2007**, *129*, 7492–7493.

(31) Asanuma, H.; Noguchi, H.; Uosaki, K.; Yu, H.-Z. *J. Phys. Chem. B* **2006**, *110*, 4892–4899.

H₂SO₄ and 30% H₂O₂) at 90 °C for 30 min. CAUTION: “Piranha” solution reacts violently with organic materials; it must be handled with extreme care. After copious rinsing with deionized water, the wafers were etched in deoxygenated NH₄F (40% aqueous solution) to remove the native oxide and obtain hydrogen-terminated silicon ($\equiv\text{Si-H}$). The fresh $\equiv\text{Si-H}$ samples were transferred under argon into Schlenk tubes containing 2–3 mL of a deoxygenated mixture of 1-decene and undecylenic acid (9:1 molar ratio) and heated at 160 °C for 3.5 h. The modified silicon samples were then rinsed at room temperature with THF and 1,1,1-trichloroethane. Esterification of the carboxyl groups with NHS was carried out by exposing the sample to a phosphate buffer (pH 6.5) containing 0.2 M NHS and 0.6 M EDC for approximately 2 h; the surface was then rinsed with water.

Amine-functionalized DNA (5'-NH₂-C₆-TCGATCTGACGT-CAGTCAA-3') in 50 mM HEPES [4-(2-hydroxyethyl)-1-piperazineethanesulfonic acid] buffer and 20 mM saline solution (NaCl, KCl, CaCl₂, or MgCl₂) was reacted with NHS-terminated monolayers on silicon for 4 h. After immobilization, the surface was washed with 2% Tween 20 in HEPES and water. Hybridization was carried out with cDNA (3'-AGCTAGACTGCAGTCAGTTT-5') in the same buffer overnight at room temperature. After hybridization, the surface was washed thoroughly with the HEPES buffer and water.

2.3. Surface Characterization. The SFG setup utilized a picosecond Nd:YAG laser (PL2143B, Ekspla) to pump an optical parametric generation/optical parametric amplification/difference frequency generation (OPG/OPA/DFG) system. The produced tunable infrared radiation is in the range of 2.3–8.5 μm .³¹ The second harmonic output of the YAG (yttrium–aluminum–garnet) laser at 532 nm was used as source of the visible light. The two beams were loosely focused onto the sample at an incident angle of 70° for visible and 50° for infrared light. The Si(111) sample was placed on the stage with the [2 $\bar{1}$ 1] direction set in the plane of the incident beams. The produced SFG beam was filtered through irises and a monochromator (Oriel Instruments, MS257) and detected by a photomultiplier tube (PMT: Hamamatsu, R3896). The SFG, visible, and IR beams were all p-polarized (abbreviated as ppp) and the SFG signal was normalized to the intensities of the visible and infrared light. All the measurements were carried out in air at room temperature (22 \pm 2 °C).

The following equations were used to express the SFG intensity (I_{SFG}):

$$I_{\text{SFG}}(\omega_{\text{SFG}} = \omega_{\text{IR}} + \omega_{\text{vis}}) \propto \left| \chi_{\text{eff}}^{(2)} : E(\omega_{\text{IR}})E(\omega_{\text{vis}}) \right|^2 \quad (1)$$

$$\chi_{\text{eff}}^{(2)} = \left| \chi_{\text{NR}}^{(2)} \right| e^{i\varphi_n} + \sum \frac{A_n}{\omega_{\text{IR}} - \omega_n + i\Gamma_n} \quad (2)$$

where $\chi_{\text{eff}}^{(2)}$ and $\chi_{\text{NR}}^{(2)}$ are the effective second-order nonlinear susceptibilities of the resonant and nonresonant components, respectively; φ_n is the phase angle between the resonant and nonresonant components; and A_n and Γ_n are the amplitude and homogeneous width of the surface vibration mode (n) corresponding to frequency ω_n , respectively. Based on the above equations, a nonlinear least-squares routine was developed in our laboratory to fit the SFG spectra.^{32–34} The quality of the fit is judged by r^2 values that were at least 0.900. Specifically, for each vibrational band the fitting parameters were A_n , ω_{IR} , and Γ_n , while $\chi_{\text{NR}}^{(2)}$ and ϕ_n were kept constant for the entire spectrum. Another parameter (a constant) was added to adjust the baseline, although this term does not influence the spectral features as it is not frequency-dependent. In principle, the nonresonant term $\chi_{\text{NR}}^{(2)}$ can affect the spectral features

as well as the baseline; however, nonresonant background from the silicon substrate is independent of the IR frequency in the spectral range 2800–3000 cm^{-1} .³³ In the cases of fitting weak or overlapped bands, ω_{IR} and Γ_n were fixed first; their initial values were obtained either from a spectrum with well-resolved bands or from the literature.^{31,33,34} The obtained amplitude of the vibration mode (A_n) was used to calculate peak intensity ratios; the uncertainties were derived from at least three individual spectra of independent samples.

X-ray photoelectron spectroscopy (XPS) measurements were carried out with a Rigaku XPS-7000 spectrometer with an Mg K X-ray source (1253.9 eV). The takeoff angle was 45° with respect to the sample surface. The pressure during analysis was $\sim 5 \times 10^{-7}$ Pa and all the peaks were normalized to the Si-2p peak (99.5 eV). Wetting measurements were performed with an AST Optima contact angle system at ambient conditions (18–22 °C, 30–35% relative humidity) where a horizontal light beam was used to illuminate the 2.0- μL water droplet. Ellipsometric measurements were made with an Uvisel spectroscopic ellipsometer (Horiba Jobin Yvon) over the range 300–700 nm at an incident angle of 70°. All experimental uncertainties reported for wetting, ellipsometric, and SFG measurements are derived from at least three independent samples.

3. Results and Discussion

Structure of the Linker Monolayer. To immobilize DNA probe strands on an oxide-free silicon surface, a linker monolayer terminated with carboxylic acid groups was prepared first (Scheme 1). It has been shown that the monolayer prepared from a 9:1 binary mixture of 1-decene and undecylenic acid provides an optimal surface density ($\sim 2 \times 10^{-11}$ mol/cm²) of acid groups for the immobilization of DNA probes,³⁵ if high hybridization efficiencies are desired.

It is essential to examine the structural properties of such linker monolayers before the surface activation and the subsequent attachment of DNA probes. Figure 1a shows the SFG spectrum of the linker monolayer prepared from a mixture of 1-decene and undecylenic acid (9:1); it resembles the spectral features of a densely packed and well-oriented $\equiv\text{Si}-(\text{CH}_2)_9-\text{CH}_3$ monolayer (Figure 1b).^{31,32} Both spectra are dominated by the characteristic peaks of the terminal methyl ($-\text{CH}_3$) groups: CH symmetric stretch (ν^+), Fermi resonance of ν^+ and CH bending overtone, and CH asymmetric stretch (ν^-) at ~ 2878 , ~ 2940 , and ~ 2964 cm^{-1} , respectively. The strong contributions from CH₃ groups and the absence of methylene- ($-\text{CH}_2-$) related peaks confirm that the mixed monolayer is well packed with an all-trans configuration of the alkyl chains.^{31–34} Furthermore, the thickness of the mixed monolayer (11.9 \pm 0.6 Å) is similar to that of $\equiv\text{Si}-(\text{CH}_2)_9-\text{CH}_3$ (11.8 \pm 1.0 Å) alone, indicating comparable surface densities as well as average tilting angles of Si–C-bonded monolayers.³⁶ The presence of carboxyl groups was confirmed by wetting measurements: the mixed monolayer exhibited much lower water contact angles (92.1° \pm 1.3°) than the $\equiv\text{Si}-(\text{CH}_2)_9-\text{CH}_3$ monolayer (108.6° \pm 0.9°). All thickness and wetting data are summarized in Table 1 for direct comparison.

Upon NHS/EDC treatment to convert the carboxyl to NHS ester groups, weak symmetric (d^+) and asymmetric (d^-) CH₂ peaks arose at ~ 2850 , ~ 2920 , and ~ 2902 cm^{-1} (Figure 1c). The former two bands are attributed to trans–gauche defects in the overall ordered alkyl chains and the latter to the CH₂ adjacent to the NHS ester group.³¹ The appearance of

(32) Ye, S.; Nihonyanagi, S.; Uosaki, K. *Phys. Chem. Chem. Phys.* **2001**, *3*, 3463–3469.

(33) Nihonyanagi, S.; Miyamoto, D.; Idojiri, S.; Uosaki, K. *J. Am. Chem. Soc.* **2004**, *126*, 7034–7040.

(34) Ishibashi, T.; Ara, M.; Tada, H.; Onishi, H. *Chem. Phys. Lett.* **2003**, *367*, 376–381.

(35) Fabre, B.; Hauquier, F. *J. Phys. Chem. B* **2006**, *110*, 6848–6855.

(36) Linford, M. R.; Fenter, P.; Eisenberger, P. M.; Chidsey, C. E. D. *J. Am. Chem. Soc.* **1995**, *117*, 3145–3155.

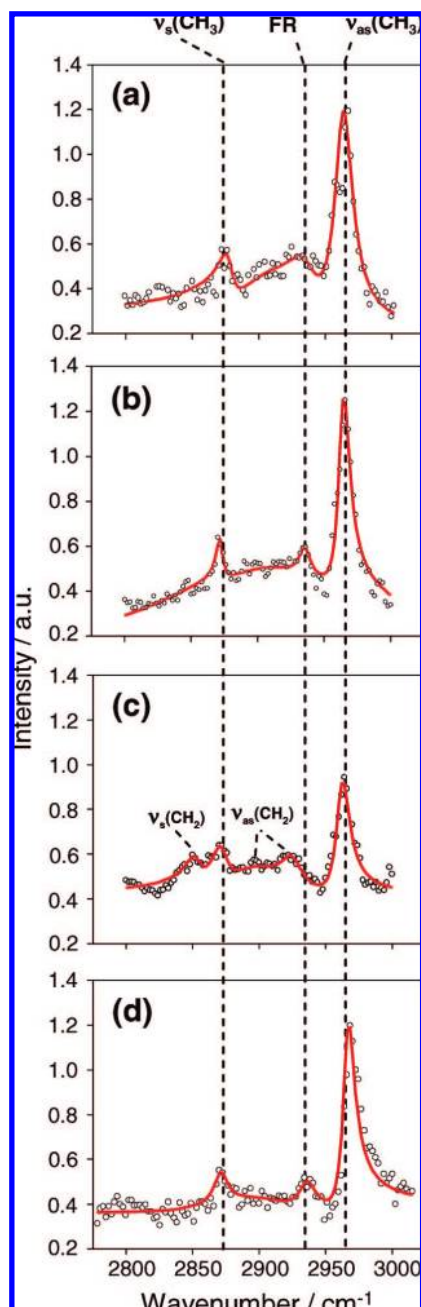


Figure 1. SFG spectra of (a) C10 monolayer, $\equiv\text{Si}-(\text{CH}_2)_9-\text{CH}_3$; (b) mixed monolayer, $\equiv\text{Si}-(\text{CH}_2)_9-\text{CH}_3/\equiv\text{Si}-(\text{CH}_2)_{10}-\text{COOH}$ (9:1); (c) mixed monolayer after formation of NHS ester; and (d) C10 monolayer upon NHS/EDC treatment (control).

Table 1. Thickness and Wetting Measurements for Control, Linker, and ssDNA Monolayers on Silicon and Effects of Different Metal Cations

sample	θ (H ₂ O)	d_{ellips} (Å)
$\equiv\text{Si}-(\text{CH}_2)_9-\text{CH}_3$ (C10)	108.6 ± 0.9	11.8 ± 1.0
$\equiv\text{Si}-(\text{CH}_2)_9-\text{CH}_3/\equiv\text{Si}-(\text{CH}_2)_{10}-\text{COOH}$ (linker)	92.1 ± 1.3	11.9 ± 0.6
$\equiv\text{Si}$ -linker-ssDNA (Na ⁺)	61.1 ± 3.4	32.9 ± 3.7
$\equiv\text{Si}$ -linker-ssDNA (K ⁺)	64.7 ± 2.8	30.1 ± 2.8
$\equiv\text{Si}$ -linker-ssDNA (Ca ²⁺)	58.8 ± 2.4	27.0 ± 2.6
$\equiv\text{Si}$ -linker-ssDNA (Mg ²⁺)	54.7 ± 2.7	26.5 ± 0.7

trans-gauche CH₂ vibrations in the backbone alkyl chains indicates the introduction of structural disorder upon surface activation, which may be due to spatial crowding during NHS

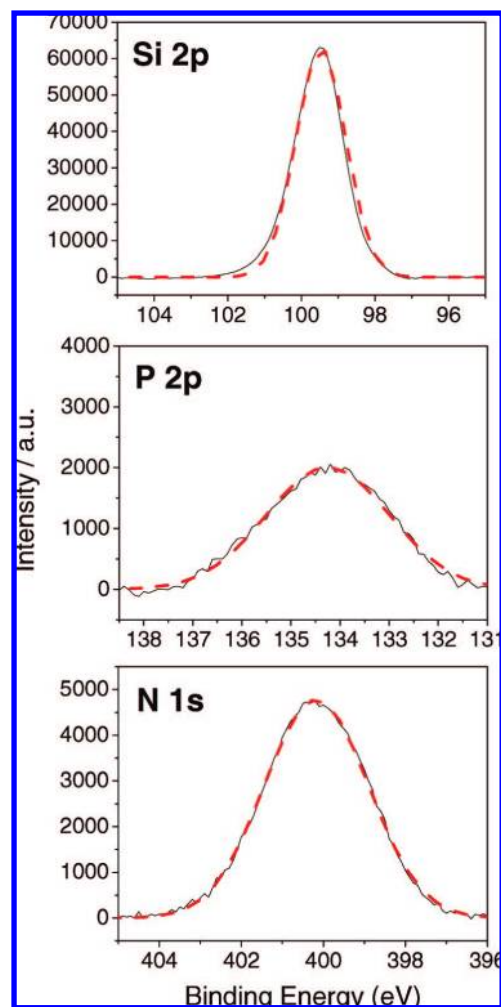


Figure 2. High-resolution XPS spectrum of DNA SAM on silicon prepared in the presence of 20 mM Na⁺. All peaks were fitted with Gaussian profiles that are shown as dashed lines in red.

ester formation via a bulky intermediate³⁷ or to the oxidation of silicon induced by prolonged incubation in an aqueous environment. In order to determine the origin of this structural change, we carried out a control experiment with a $\equiv\text{Si}-(\text{CH}_2)_9-\text{CH}_3$ sample that was treated with NHS/EDC for 2 h under the same conditions as the surface activation of mixed monolayers (Figure 1b). The resulting SFG spectrum (Figure 1d) showed that methylene-related peaks were negligible and the general features were virtually identical. We have therefore confirmed that the disruption of the mixed monolayer structure upon activation is not due to oxidation or damage of the silicon substrate; rather, it relates directly to the surface reactions of carboxyl groups.

Immobilization of DNA Strands. Silicon surfaces upon immobilization of DNA strands were first analyzed by XPS to confirm the coupling reaction. Since phosphate (P) and nitrogen (N) peaks are typically not influenced by surface contamination, they (particularly P peaks) constitute good evidence for the presence of DNA strands on the surface. Samples prepared in the presence of different cations all exhibited identical XPS profiles. Representative high-resolution spectra in the Si 2p, N 1s, and P 2p regions are shown in Figure 2. The P 2p peak

(37) Sehgal, D.; Vijay, I. K. *Anal. Biochem.* **1994**, *218*, 87–91.

observed at 134.3 eV is consistent with that reported for the phosphate backbone of DNA.^{38,39} The high-resolution spectrum exhibited a single peak at 99.5 eV for Si 2p. The slight deviation of this peak from Gaussian shape is an indication of surface oxidation. However, the absence of peaks at higher binding energies indicates that passivation with an organic monolayer minimizes the oxidation of silicon during surface activation and DNA immobilization. The -NH- group in the linker and the nonconjugated nitrogens of DNA are represented by the N 1s peak at 400.2 eV, which has been reported to be the characteristic signal of nonconjugated nitrogen.⁴⁰ No N 1s peak corresponding to N–O (402.6 eV)¹⁹ was observed, indicating efficient amide coupling of amine-functionalized DNA to the surface carboxyl groups (Scheme 1).

The significant decrease in water contact angles and increase in the monolayer thickness (Table 1) observed upon DNA immobilization are additional proof for the covalent anchoring of DNA strands on the silicon surface, as they are intrinsically hydrophilic molecules. Our thickness data are comparable to those reported in the literature,⁴¹ yet substantial differences have been observed among DNA SAMs prepared in the presence of different cations. These results are elaborated in the following section.

Structure of DNA SAMs and Effects of Cations. In order to compare the effects of different cations on the formation and reactivity of DNA SAMs on silicon, 20 mM NaCl, KCl, CaCl₂, or MgCl₂ was added to the buffer used in the surface coupling and hybridization steps (50 mM HEPES, pH 7.2). The SFG spectra of the silicon surfaces upon DNA immobilization and subsequent hybridization are summarized in Figure 3. Trans-gauche defects are observed in all cases: that is, methylene-related peaks became evident, and methyl bands were considerably weakened. Nevertheless, several spectral features differed discernibly from each other for the four ssDNA samples prepared in the presence of different cations: with Na⁺ (top of Figure 3a) and K⁺ (top of Figure 3b), the linker monolayers were less disordered than those prepared with Ca²⁺ (top of Figure 3c); the latter were characterized by more intense methyl peaks. Mg²⁺ ions had the most significant effect (top of Figure 3d): in this case the CH₃ bands became weaker than the CH₂ peak intensities.

A quantitative estimate of the number of gauche defects in the alkyl chains could not be easily obtained. However, the CH₃/CH₂ peak intensity ratio (r^-/d^-) provides a good measure of the molecular order within an organic monolayer: the higher the ratio, the more ordered the alkyl chains.²⁷ Based on the spectra shown in Figure 3 (top spectrum of each panel), this value was found to be 1.8 ± 0.2 for a sample exposed to Na⁺, 1.8 ± 0.1 for K⁺, 1.4 ± 0.2 for Ca²⁺, and 0.7 ± 0.3 for Mg²⁺. Thus, the distortion of the linker monolayer decreased in the order Mg²⁺ > Ca²⁺ > Na⁺ ≈ K⁺. Such a trend is strikingly akin to the affinities of metal cations for nucleic acids: divalent cations bind much more strongly than monovalent cations.¹³ However, there are contradictory reports regarding the affinities of Mg²⁺ and Ca²⁺ for DNA.^{13,14} We have, therefore, carried

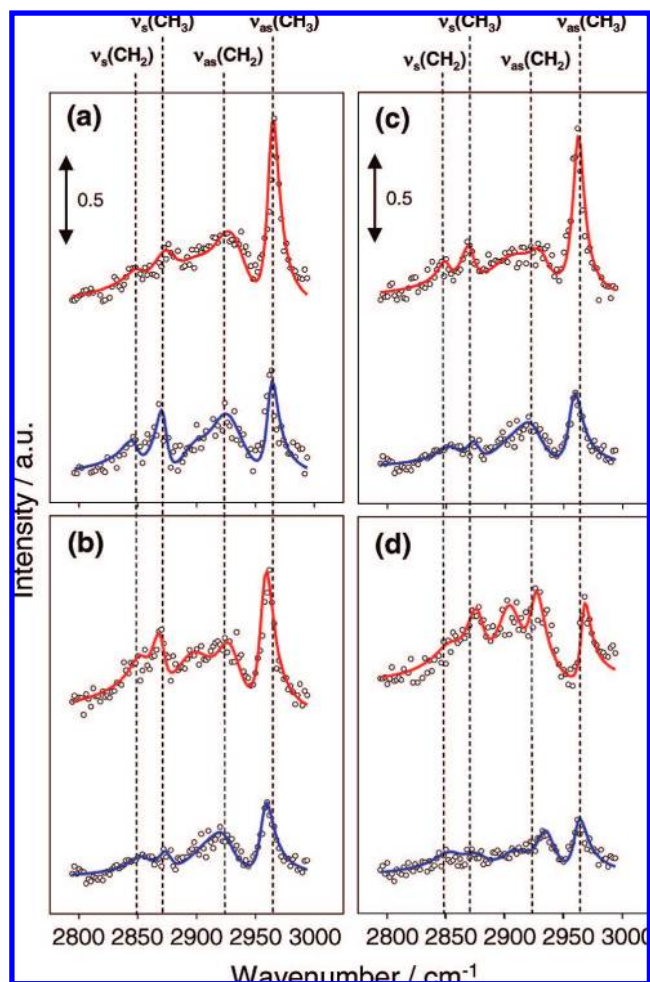


Figure 3. SFG spectra of silicon modified with DNA SAMs prepared in the presence of 20 mM (a) NaCl, (b) KCl, (c) CaCl₂, and (d) MgCl₂. In each panel, the top spectrum (red fitting line) is from the activated silicon surface upon immobilization of probe strands (ssDNA SAMs on silicon), and the bottom spectrum (blue fitting line) is that after hybridization (dsDNA SAMs on silicon).

out XPS studies to further elucidate the differences between these two divalent cations.

As shown in Figure 4, Ca²⁺ and Mg²⁺ were both observed in the ssDNA SAMs as evidenced by the Ca 2p (342 eV) and Mg 2p peaks. The Mg 2p spectrum had to be deconvoluted into two peaks at 52.0 and 55.0 eV to obtain the best fit (Figure 4a), indicating that there are at least two distinctive sites for Mg–DNA interaction: the negatively charged phosphate backbone (higher energy), and the nucleoside units (lower energy) for hydrated Mg²⁺ ions are known to interact with DNA bases by hydrogen bonding.¹ Compared to Ca²⁺, Mg²⁺ existed more persistently within the monolayer as evidenced by the cation/phosphate signal ratio (normalized by the respective sensitivity factor of the XPS measurements): the Mg/P value was estimated to be 1.45, much higher than that of the Ca/P peaks (0.04). We believe that such a large difference is not due to differences in their binding constants⁴² but rather to different exchange rates with other cations present in the medium (i.e., washing buffer). Ray et al.⁴¹ have reported that the concentration of cations within DNA monolayers decreases quickly upon proton exchange.

Upon hybridization, only a trace of the Mg signal was observed (Figure 4c), and the signal for Ca was negligible

(38) Lee, C. Y.; Gong, P.; Harbers, G. M.; Grainger, D. W.; Castner, D. G.; Gamble, L. J. *Anal. Chem.* **2006**, *78*, 3316–3325.

(39) Petrovykh, D. Y.; Kimura-Suda, H.; Tarlov, M. J.; Whitman, L. J. *Langmuir* **2004**, *20*, 429–440.

(40) Sapirgin, A. V.; Thomas, C. W.; Dulcey, C. S.; Patterson, C. H.; Spector, M. S. *Surf. Interface Anal.* **2005**, *37*, 24–32.

(41) Ray, S. G.; Cohen, H.; Naaman, R.; Rabin, Y. *J. Am. Chem. Soc.* **2005**, *127*, 17138–17139.

(42) Su, L.; Sen, D.; Yu, H.-Z. *Analyst* **2006**, *131*, 317–322.

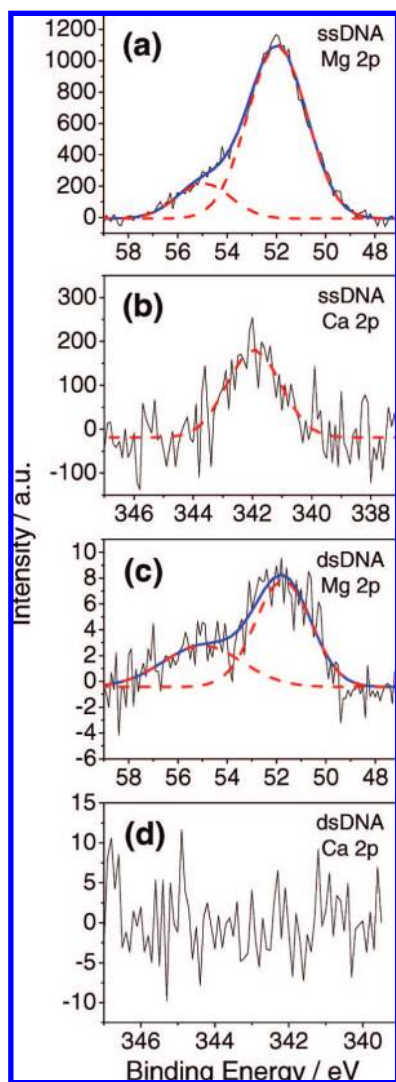
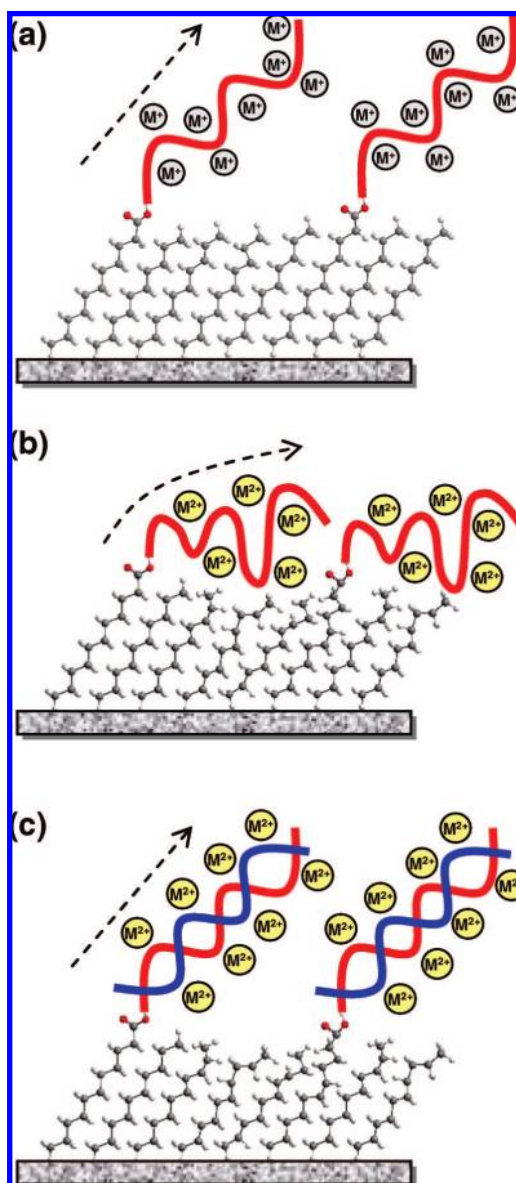


Figure 4. XPS spectra of silicon modified with DNA SAMs upon immobilization in the presence of 20 mM (a) MgCl_2 or (b) CaCl_2 and after hybridization with complementary strands in the presence of 20 mM (c) MgCl_2 or (d) CaCl_2 . All peaks were fitted with Gaussian profiles. The Mg 2p spectrum was deconvoluted into two peaks (red dashed lines), suggesting that there are two types of interaction sites within DNA.

(Figure 4d). Monovalent cations were not observed in the XPS spectra of either single- or double-stranded DNA SAMs on silicon as previously reported,⁴¹ where the “shortage” of cations to neutralize the DNA may be compensated by the adsorption of protons. Furthermore, differences in persistence among cations are exhibited in wetting measurements (Table 1). The water contact angles of ssDNA SAMs prepared in the presence of different cations increased in the order Mg^{2+} ($54.7^\circ \pm 2.7^\circ$) < Ca^{2+} ($58.8^\circ \pm 2.4^\circ$) < Na^+ ($61.1^\circ \pm 3.4^\circ$) < K^+ ($64.7^\circ \pm 2.8^\circ$). Such a decrease in surface hydrophilicity can be explained by differences in the number of cations trapped within the DNA monolayer on silicon.

To explain the correlation between degree of deformation of the linker monolayer and DNA–cation affinities ($\text{Mg}^{2+} > \text{Ca}^{2+} > \text{Na}^+ \approx \text{K}^+$), the effect of the cations on the conformations of DNA strands must be considered. DNA is a locally stiff molecule but uneven “neutralization” of the charge of the phosphate backbone could be a significant driving force for conformational change.³ Since the most frequent interactions between metal cations and DNA occur at the guanine bases,

Scheme 2. Hypothetical Representation of Cation-Induced Structural Changes of DNA/Linker Monolayer on Silicon Surface^a



^a (a) In the presence of monovalent cations, the geometry of DNA is unaffected and the underlying linker monolayer keeps its ordered conformation. (b) Divalent cation-induced DNA deformation significantly perturbs the linker monolayer. (c) Hybridization in the presence of divalent cations does not introduce further disruption to the linker monolayer structure.

the distribution of cations around the DNA molecule is not uniform, causing DNA strands to curve and bend substantially on the surface. Deformation of the DNA SAMs is expected to be more significant as DNA–cation interactions become stronger, which would explain the fact that Mg^{2+} ions disrupt the SAM structure more effectively than sodium or potassium ions. If such distortion is significant enough, it will likely affect the lateral order of the underlying linker monolayer (Scheme 2).

We therefore conclude that the perturbation to the structure of the linker monolayer results from the deformation (curving and bending) of DNA strands on the surface induced by their interactions with metal cations in solution: the r^-/d^- ratio reflects the degree of such structural deformation. Accordingly, the lowest r^-/d^- ratio (0.7 ± 0.3) measured in the presence of Mg^{2+} is an indication of substantially deformed DNA SAMs, while

Ca^{2+} has a smaller effect. Our results show that the deformation of ssDNA SAMs caused by millimolar concentrations of Na^+ or K^+ is negligible, certainly insufficient to disrupt the underlying alkyl chains (Scheme 2a). Prior to DNA immobilization, the r^-/d^- ratio was 1.9 ± 0.2 (Figure 1c), which is virtually identical to that of a DNA monolayer prepared in the presence of 20 mM Na^+ or K^+ (top spectra of Figure 3a,b).

The remarkable difference between the conformational orders of ssDNA SAMs prepared with different cations is also supported by ellipsometric measurements (Table 1). Layer thickness correlated well with DNA–cation affinity: Mg^{2+} ($26.5 \pm 0.7 \text{ \AA}$) < Ca^{2+} ($27.0 \pm 2.6 \text{ \AA}$) < K^+ ($30.1 \pm 2.8 \text{ \AA}$) \approx Na^+ ($32.9 \pm 3.7 \text{ \AA}$). As the affinity increases, the layer thickness decreases. Bend and curvature will shorten the length of the DNA strands, thus the layer thickness should decrease accordingly as the deformation becomes more significant.

Upon hybridization in the presence of monovalent cations, the linker monolayer structure becomes more disordered (bottom of Figure 3a,b): the r^-/d^- value dropped to 1.2 ± 0.2 and 1.3 ± 0.1 for Na^+ and K^+ , respectively. However, in this case the extent of further structural disruption is not as significant as in the immobilization step. Molecular dynamics simulations have indicated that DNA double helices tethered on chips have minimal contacts with the surface and point mostly into the solution,^{43,44} therefore the disruptions, most likely due to spatial restraints during incorporation of the complementary strands, are “transferred” to the underlying alkyl chains. In the presence of divalent cations, the r^-/d^- ratio was not affected as much (bottom of Figure 3c,d: 1.2 ± 0.3 and 0.8 ± 0.2 for Ca^{2+} and Mg^{2+} , respectively). There are mainly three regions where metal cations interact with double-stranded DNA: the phosphate backbone, the major grooves, and the minor grooves.¹¹ Monovalent cations bind preferentially in the minor grooves of an AT tract,² whereas Mg^{2+} and Ca^{2+} coordinate with both the major and minor grooves.⁴⁵ While such preferential binding certainly induces structural deformation of both ssDNA and dsDNA SAMs on silicone, our experimental data support the view that it does not influence the conformation of dsDNA monolayers as much as that of ssDNA SAMs. DNA double helices are much stiffer than ssDNA and will maintain well-oriented conformations with minimum DNA–surface interactions,^{43,44} which are not influenced significantly by the presence of divalent cations. In fact, the divalent cations would reduce the repulsion between the DNA strands,⁴ thereby facilitating hybridization in a more confined space and minimizing disruption of the underlying linker layers. Overall, the hybridization process has a small influence on the lateral order of the linker monolayer (Scheme 2c), although it does not reverse to the original ordered packing.

We have elaborated the influence of metal cations on the conformation of DNA strands on silicon and concluded that their effect on the hybridization process is the origin of the conformational changes in the linker monolayers. Our postulate is based on SFG data (Figure 3), showing that the extent of such distortion of the alkyl chains parallels the order of cation–DNA affinities. However, there is another possible

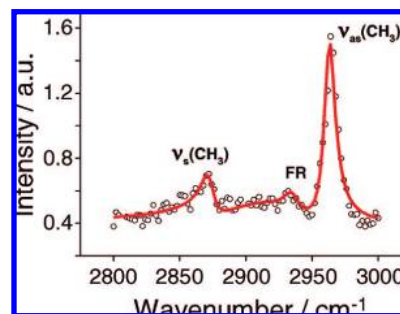


Figure 5. Representative SFG spectrum of the mixed monolayer on silicon prepared from 1-decene/undecylenic acid (9:1) treated with 20 mM MgCl_2 overnight.

cause: the interaction between positively charged ions, especially relatively soft ions such as Ca^{2+} , and underlying unreacted carboxyl groups may be strong enough to induce the observed deformation of the linker layer. To exclude this possibility, a control experiment was carried out with mixed monolayers formed from 1-decene and undecylenic acid (molar ratio 9:1) incubated in 20 mM NaCl , KCl , CaCl_2 , or MgCl_2 overnight. None of the cations caused significant changes in the SFG spectra of monolayer-modified silicon surfaces. As shown in Figure 5, even after prolonged incubation in Mg^{2+} solutions, the features of a well-ordered linker monolayer are retained: strong intensity of methyl bands and negligible methylene peaks. Therefore, we can conclude that the disruption of linker monolayer structure is predominantly induced by deformation of the DNA SAMs.

4. Conclusion

The effect of metal cations on the formation of ssDNA SAMs on silicon and on the hybridization process is significant. Our SFG investigation confirms semiquantitatively that the extent of structural distortion parallels the order of metal ion–DNA affinities. The trend was opposite during hybridization when further disruption of the underlying linker monolayer was greater for monovalent cations (Na^+ and K^+), indicating that divalent metal cations (in particular Mg^{2+}) facilitate hybridization in a more spatially confined manner. We have provided herein the first spectroscopic evidence for cation-induced conformational changes of DNA strands on surfaces. Such information is critical for the preparation of DNA microarrays with optimal probe density and molecular conformation, which affects on-chip hybridization efficiency.

Acknowledgment. We are grateful to the Natural Science and Engineering Research Council of Canada for financial support. This work was also supported by Promotion of Novel Interdisciplinary Fields Based on Nanotechnology and Materials, the Global COE Program (Project B01: Catalysis as the Basis for Innovation in Materials Science), and Grants-in-Aid for Young Scientists (B) (19750054) and for Scientific Research (A) (18205016) from the Ministry of Education, Culture, Sports, Science and Technology (MEXT), Japan. H.A. is grateful for the help received from Hitoshi Fukumitsu for some of the experiments and thanks Mikio Ito and Tsubasa Okada for fruitful discussions. We thank Dr. Eberhard Kiehlmann for critically reading and editing the manuscript.

JA801023R

(43) Wong, K.-Y.; Pettitt, M. B. *Theor. Chem. Acc.* **2001**, *106*, 233–235.

(44) Wong, K.-Y.; Pettitt, M. B. *Biopolymers* **2004**, *73*, 570–578.

(45) Minasov, G.; Tereshko, V.; Egli, M. *J. Mol. Biol.* **1999**, *291*, 83–99.